PAPER

Check for updates

Ultrafast, scalable laser photothermal synthesis and writing of uniformly dispersed metal nanoclusters in polymer films†

Pankaj Ghildiyal, [ID] [a,c] Yong Yang, [ID] [b,c] Dylan J. Kline, [ID] [b,c] Scott Holdren[a] and Michael R. Zachariah [ID] *[c]

This paper presents a fast CO_2 laser synthesis and writing technique – laser photothermal synthesis and writing (LPSW) – to generate and write a high concentration of unaggregated, spherical sub-10 nm metal nanoparticles (sMNPs). The method is generic, and we demonstrate the fabrication of Ni, Cu, and Ag directly in polymer thin films. A partly IR-absorbing thin polymer film can be heated by the laser to high temperatures in a short time, triggering metal-reduction, nucleation, and growth. Rapid quenching of polymer films suppresses particle diffusion and traps the generated sMNPs in the polymer film. As a result, these particles are immobilized in the laser illuminated spot ("written" by the laser) on quenching. Here, Ag–polymer films are used as a model to demonstrate how laser parameters – pulse duration, laser energy flux, and number of pulses (pulsed thermal load) – can be varied to tune particle size distributions of metal sMNPs. Using this approach, we have been able to generate 4–12 nm Ag sMNPs with thermal pulses as short as 35 ms. Fast heating timescales employed in this approach allow for the scalable manufacturing of high yields of metal sMNPs, which we estimate to be around 1 g min^{-1}. This rapid, general synthesis and writing technique may have potentially important applications in fast, large-scale additive manufacturing and patterning of metal-loaded polymer multilayers, flexible electronics, and sensors.

1. Introduction

Small metal nanoparticles (sMNPs) with dimensions less than 10 nm have unique optical, electronic, and catalytic properties that are highly sensitive to particle size and shape.[1,2] These properties make them ideal candidates for tunable materials in applications ranging from high-efficiency catalysts,[3,4] fluorescence bioimaging,[5] antimicrobial agents,[6] energetic materials,[7] and sensors.[8,9] Although colloidal science has achieved unprecedented control over the shape and size of

metal nanoparticles, generating a high-density of such particles in a scalable and continuous manner is still a challenge for nanoscience. Colloidal techniques commonly used to synthesize sMNPs include sol–gel,[10] electrochemical,[11] sonochemical,[12] and polyol approaches.[13,14] These techniques nominally have slow kinetics, typically in the order of several hours and often suffer from particle agglomeration and inhomogeneous growth when the reaction volumes are scaled up. Tuning of the size is often achieved with surfactants and capping agents.[12,13] An ideal, scalable method would be one where the particle size and properties of SMNPs can be tuned by modulating the parameters of an automatable instrument, instead of relying on external agents such as surfactants and capping ligands as most colloidal techniques do. Additionally, for many potential applications, nanoparticles might be desired with not only size control but also with well-defined spatial distribution. This latter possibility is particularly attractive as we move to a 3-D additive manufacturing setting.

Lasers offer a versatile next-generation tool to produce pulsed, spatially resolved energy to drive chemical reactions, which can be employed to trigger nanoparticle formation. Laser based lithography techniques shift the control and modulation of properties from the material to a programmable instrument. Recently, a number of laser-based fabrication

[a] Department of Chemistry and Biochemistry, University of Maryland, College Park, MD 20742, USA

[b] Department of Chemical and Biomolecular Engineering, University of Maryland, College Park, MD 20742, USA

[c] Department of Chemical and Environmental Engineering, University of California, Riverside, CA 92507, USA. E-mail: mrz@engr.ucr.edu

†Electronic supplementary information (ESI) available: Finite element simulation details; selected area electron diffraction patterns and X-ray diffraction analysis of metal-PVA films; number of particles counted for PSD analyses; large area TEM images of uniformly dispersed Ag sMNPs in PVA thin films; effect of substrate characteristics on PSD; calculation of the production rate of metal sMNPs; lateral heat diffusion and thermal damage to polymer films in laser writing; dispersibility of laser-written metal nanocluster-polymer films in solution. See DOI: 10.1039/c9nr02839k

strategies for metal nanostructures have been explored, the most popular of which include laser ablation in gas and liquid phases,[15,16] laser direct synthesis and patterning (LDSP),[17] and direct laser writing (DLW)[18] among others. Laser ablation techniques use a top-down approach to thermally evaporate metal targets followed by condensation either in air or liquid solvents to generate metal nanoparticles. High diffusion rates in gas and liquid media lead to random uncontrollable growth, nanoparticle sintering, and broad size distributions. On the other hand, DLW uses laser beams tightly focused on a photosensitive material to photochemically generate nano- and micro-structures. However, these processes are limited to generate structures of only Ag as photosensitive inks are required in these methods.[18,19] To generalize these processes to other metals, an alternative approach could be to use the laser photothermal effect to induce particle formation. Polymer thin films have been demonstrated to be effective host matrices for the *in situ* fabrication of sMNPs.[20,21] These matrices are able to immobilize and stabilize sMNPs from aggregation. Although these techniques generate uniform dispersions of sMNPs effectively, the methods explored so far are conventional, slow oven-heating techniques and have been mostly restricted to easy-to-reduce metals such as Au, Ag, and Pd.[20–23]

Here, we provide an alternative hybrid technique that combines the scalability and precision of lasers with the generality and flexibility of traditional thermal techniques used in colloidal synthesis. We demonstrate a novel approach, termed laser photothermal synthesis and writing (LPSW), that uses laser induced localized polymer heating to *in situ* generate small, high-density, monodisperse, unaggregated sub-10 nm metal nanoparticles directly in polymer thin films. A continuous wave CO_2 laser operating at mid-IR frequency (10.6 μm) is chosen as the heating source as most polymers have partial vibrational absorption in this spectral region, allowing for the flexibility of the laser to work with a range of plastics. This technique follows a simple protocol for sample preparation using readily available metal nitrate precursors to form metal-precursor–polymer thin films. Since IR does not nominally have sufficient energy to induce photochemical transformations, absorption in the polymer results primarily in thermal excitation over a short time frame. This localized fast heating triggers metal atom-forming reduction reactions and subsequent nucleation, while fast quenching slows down particle diffusion and freezes the formed particles in the polymer matrix. In this way, the polymer matrix has multiple roles in this process – a medium to incorporate dissolved metal salts, photothermal sensitizer to induce particle formation, and a stabilizing matrix to suppress the diffusion and coagulation of the resulting sMNPs. Fig. 1 shows the experimental setup and various processes occurring in the polymer matrix. Shock heating to a high temperature for a short time induces a large supersaturation of metal atoms in the polymer matrix, resulting in burst nucleation. During this heating period, multiple processes occur in the matrix: (i) metal-ions get reduced to zero-valent metal atoms, (ii) polymer viscosity decreases allowing for partial diffusion of metal atoms through the matrix followed by nucleation, (iii) as metal nuclei grow larger, their diffusion slows down. As a result, particles of a certain size are formed.

Here, we use the term "writing" in this fabrication technique as the particles formed are frozen in the matrix after the laser is turned off. In other words, the particles in the matrix
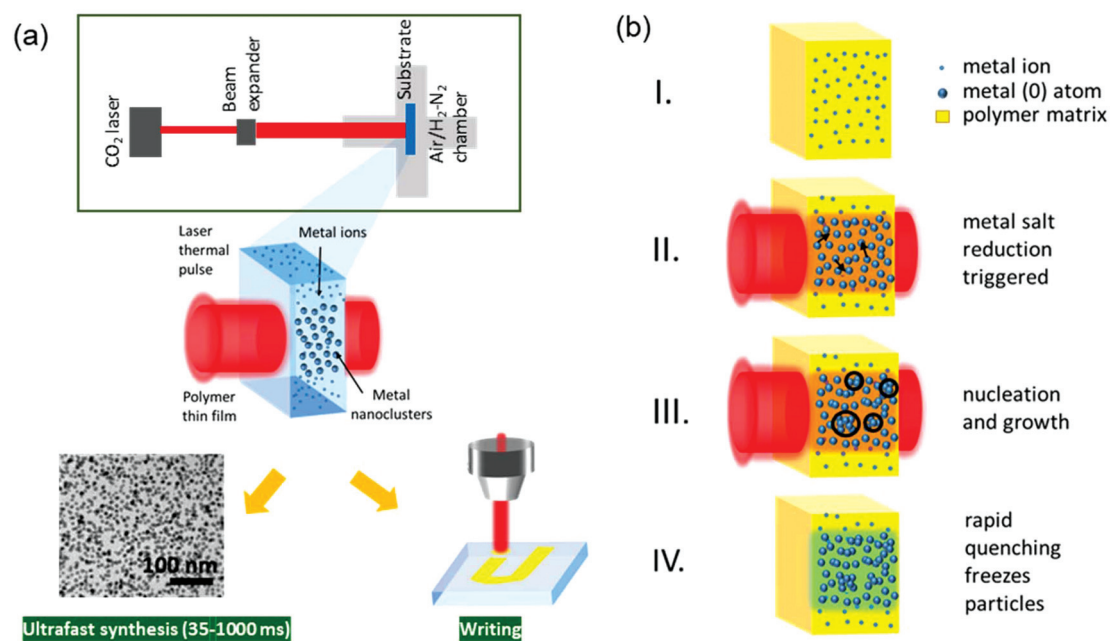
Fig. 1 (a) Schematic showing the laser photothermal synthesis and writing (LPSW) to form small metal nanoclusters directly in the polymer thin film. (b) Basic mechanism of nanocluster formation by LPSW.

stay immobilized at the same spot where the laser beam hit the polymer. Thus, different particle sizes and distributions can be obtained in a single polymer film by varying the laser parameters and moving the substrate or the laser. By using an appropriate reducing atmosphere in our chamber, we have been able to generate uniformly dispersed, relatively mono-disperse sMNPs of a variety of metals including Ag, Cu, and Ni. In this study, we have chosen Ag as a model metal to understand the growth mechanisms of sMNPs in polymer films by our technique. We demonstrate how particle size distributions can be precisely modulated by varying laser characteristics – pulse duration, laser energy flux, and number of input pulses (pulsed heat load). We further discuss the impact of critical characteristics of the polymer matrix and substrate on resulting particle size distributions. Since the polymer is only partly absorbing (ESI, Fig. S2†), the laser beam should be able to penetrate through thick or even multilayer films generating particles along its path – opening possibilities for additive manufacturing and 3-d writing of sMNPs in reactive multi-layers. To the best of our knowledge, this is the first time that immobilized, unaggregated sub-10 nm sMNPs of Ag, Ni, and Cu have been fabricated in polymer matrices by the laser heating method. We further note that our LPSW process: (a) is facile, fast, and scalable, (b) uses readily available metal nitrate salts and polymer, (c) allows for laser-controlled size and concentration of sMNPs, (d) can be used to generate arbitrary patterns of unaggregated sMNPs directly on free-standing polymer films, and (e) is general and flexible enough to synthesize high-density uniform dispersions of both noble and non-noble metals in any IR absorbing polymer matrix.

2. Experimental section

2.1. Materials

Silver nitrate (AgNO$_3$, ≥99% pure), copper nitrate trihydrate (Cu(NO$_3$)$_2$·3H$_2$O, ≥99% pure), nickel nitrate hexahydrate (Ni(NO$_3$)$_2$·6H$_2$O, ≥99% pure), PVA (MW 89k–98k and 9k–10k, ≥99% and 80% hydrolyzed, respectively), and polystyrene (MW 280 000) were purchased from Sigma-Aldrich and were used as received.

2.2. Preparation of metal precursor-polymer thin films

The metal precursor–polymer solution was prepared by dissolving PVA (1.5 g) and the desired amount of metal nitrate salt in deionized water (14 mL). The metal to polymer mass ratio was kept constant at 0.05. This mass ratio was prepared by dissolving stoichiometrically equivalent amounts of the metal salt. Larger amounts of the polymer were used to prepare thicker polymer films. The resulting metal precursor–polymer solution was then spin coated under ambient atmosphere on a clean, dry glass slide at 2000 rpm for 10 s. For large-area TEM characterization, the glass slide was first coated with a PS solution (9 g in 42 mL toluene, 700 rpm, 10 s). A metal salt–PVA solution (1.2 g PVA and a certain amount of the metal salt in 14 mL deionized water) was then spin coated on the dry PS

film to obtain a very thin PVA–PS–metal precursor film. This film was later used to fabricate PS–PVA–metal films for UV-Visible spectroscopy and microscopy analysis. All films were dried under flowing air for ~2 hours before laser synthesis.

2.3. Laser photothermal synthesis and writing

Fig. 1 shows the setup of the LPSW technique to fabricate metal–polymer thin films. In a typical experiment, glass substrates coated with metal precursor–PVA films are aligned in a direction normal to the incoming laser beam. The precursor–polymer films are then irradiated by a continuous wave CO$_2$ laser (SYNRAD, ti series) operating at 10 640 nm with a maximum output power of 80 W. A beam expander is used to expand the collimated laser beam to a spot size of 1 cm, corresponding to a maximum input laser energy flux of 25 W cm^{-2}. The setup also includes a chamber to control the atmosphere of the fabrication process. For Ag–PVA films, ambient atmosphere is used to reduce the metal. However, for more readily oxidizable metals with a lower reduction potential (Cu, Ni), the chamber is kept under flowing H$_2$ (5% in N$_2$) which acts as a reducing gas for metal ions in the polymer. PVA films are partly absorbing in the operational wavelength of the laser (FTIR spectra, ESI, Fig. S2†). Therefore, the laser beam is able to heat the polymer rapidly to very high temperatures for a relatively short duration.

The rapid thermal shock pulse triggers metal salt reduction and generates a large supersaturation of metal atoms. Decreased polymer viscosity upon heating allows for metal atom diffusion, enabling nucleation. Turning off the beam results in fast quenching which suppresses particle diffusion and freezes them in the solid polymer matrix. A beam of a fixed spot size (1 cm diameter) is used in all experiments, while laser energy flux and pulse duration are varied from 3–23 W cm^{-2} and 200–4000 ms, respectively. Furthermore, using a pulse generator, multiple heating pulses at prescribed intensities and pulse duration were implemented in periodic heat load experiments, as described later.

2.4. Characterization of metal–polymer films

UV-Visible spectra of LPSW fabricated PS–PVA–sMNP films (on glass) were recorded using a PerkinElmer Lambda 1050 UV/Vis/NIR spectrophotometer in the integrating sphere (150 mm) configuration. Metal particles in LPSW fabricated metal–PVA films were imaged by transmission electron microscopy (TEM, JEOL JEM 2100 LaB$_6$). For some samples, films were scraped off and placed on the TEM grid, and their thin edges were imaged. To obtain a direct, quantitative overall particle size distribution in a larger area, an alternative sample preparation procedure[24,25] was employed. In this method, the PS–PVA–metal precursor film (preparation described above) is used to fabricate a PS–PVA–sMNP composite film by LPSW. After laser irradiation, the thick multilayer film was cut and placed on a TEM grid, followed by immersion in toluene. The sacrificial PS layer dissolves in the solvent, while the ultrathin PVA–sMNPs stick to the grid. This film was directly imaged to assess metal

particle size distribution in the entire PVA matrix. Statistical analysis of size distribution of metal nanoparticles in the film was performed using Nanomeasurer 1.2.5 analysis software. Film thicknesses were obtained using a Hitachi SU-70 field emission gun scanning electron microscope (FESEM). Fourier transform infrared spectroscopy (ThermoFisher Nicolet iS50R spectrometer) was used in the transmission mode at 4 cm^{-1} resolution to characterize the structure and infrared absorption of the polymer. X-ray diffraction (XRD) was performed using a PANalytical Empyrean Series 2 X-ray diffractometer (Cu Kα radiation).

2.5. Finite element simulation of laser heating profiles

In order to estimate the heating profiles and peak temperatures of polymer films during the laser heating process, a finite-element simulation of the photothermal process was implemented using COMSOL Multiphysics software (v. 5.3, Build 275). The model with the polymer films and glass substrate is constructed and simplified by exploiting the symmetry of the model geometry (ESI, Fig. S1†). To model the photothermal effect and heating profiles, absorption coefficients for each layer in the system are determined by FTIR transmission spectroscopy. First, PVA and PS films with known thicknesses (from FESEM) are prepared, and a linear absorption coefficient was estimated for each by Beer's law (ESI, Fig. S2†). For the glass substrate (on which the polymer films are coated), absorption coefficient values reported in the literature are used.[26]

Assuming the absorbed IR radiation completely manifests itself non-radiatively as heat, we can treat the system as a heat-transfer problem. Heat input into the system can be modelled as a volumetric heat source (W m^{-3}) input in the following form:[27]

$$Q_{absorbed} = P_{incident} \cdot \left(\frac{\alpha}{\pi r_{laser}^2} \right) \cdot \exp\left(-\frac{x^2 + y^2}{r_{laser}^2} \right) \cdot \exp(-\alpha z) \quad (1)$$

where, $Q_{absorbed}$ is the volumetric heat input (in W m^{-3}) absorbed by the film; $P_{incident}$ is the laser power (in W) incident on the film surface; α is the linear absorption coefficient (in m^{-1}) of the film; r_{laser} is the radius of the laser spot.

Propagation of the laser beam through multiple layers (PVA, PS, and glass) is implemented as follows. Laser power transmitted (total input – absorbed power) by the previous layer becomes the incident power ($Q_{incident}$) for the subsequent layer. The absorbed power is determined using the thicknesses and absorption coefficient of individual layers. The second to last term on the right in eqn (1) simulates the Gaussian shape of the laser pulse, while the last term represents the exponential decay as a part of the laser energy input (propagating in z-direction) is absorbed by the component layer.

Both conductive and convective heat losses were included in the model; radiative heat loss was neglected due to the relatively low temperatures our system operates in. Convective heat transfer from the surrounding gas was implemented by incorporating the non-isothermal laminar flow module in the soft-

ware and coupling with the heat transfer module in the software. A free-triangular mesh was generated in the PVA thin film and was swept throughout the model. A periodic switch (on/off) function was added to the aforementioned input heat source equation to obtain quenching rates and laser pulse. Details of the model geometry, mesh elements, applied boundary conditions, and thermal property data used in the model can be found in the ESI, section S1.†

3.   Results and discussion

3.1   Formation of metal nanoclusters in polymer films by LPSW

Metal sMNP formation starts with the reactions forming zero-valent metal atoms from metal ions. A general decomposition and reduction reaction for the metal, M (Ni and Cu), from the corresponding metal salt can be written as:

$$M(NO_3)_2 + 2H_{2(g)} \xrightarrow{\Delta} M^0 + 2NO_2 \uparrow + 2H_2O \uparrow \quad (2)$$
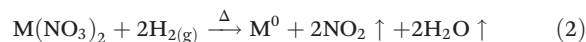
Since these metals have lower reduction potentials, thermal energy must be supplied to trigger the metal ion reduction by H_2 gas. For writing Ag into the polymer, it has been demonstrated that on heating the polymer, PVA, with Ag$^+$ salt, –OH groups in the polymer itself are able to reduce Ag$^+$ ions to Ag^0 via a polyol like reduction mechanism.[24] Although the actual reaction mechanism may be complex, the overall equation can be written as:

$$R_2CH\text{-}OH + AgNO_3 \xrightarrow{\Delta} Ag^0 + R_2CO + H_2O \uparrow + NO_2 \uparrow \quad (3)$$
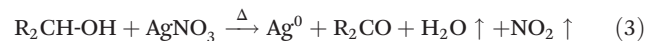
Ag, which has a high reduction potential and is stable more as Ag than Ag$_2$O, did not require synthesis under a H_2 atmosphere unlike Cu and Ni.

Fig. 2 shows unaggregated sMNPs of three metals (Ni, Cu, Ag) written directly in PVA films (coated on a 0.2 mm thick glass slide) by LPSW. In each case, the particles are relatively monodisperse (geometric standard deviation of lognormal fit, σ_g (Ag, Cu, Ni) = 1.10, 1.15, 1.17) and spherical in shape with a uniform dispersion throughout the matrix.

Selected area electron diffraction (SAD) patterns (ESI, Fig. S3†) confirm the identity of individual metals in the films. These results are further corroborated by X-ray diffraction (XRD) patterns on LSPW-fabricated, high metal-loading polymer films (ESI, Fig. S4†). This confirms that the metal ions have been reduced to the corresponding zero-valent metals.

Table 1 summarizes the operational laser and film parameters used to fabricate these films. We see that a relatively lower energy flux and short duration are sufficient to form Ag and Cu sMNPs in the polymer film. On the other hand, Ni requires much higher laser intensities and pulse duration to be reduced by H_2. The film temperature estimated from finite-element simulations for the fabrication of Ni sMNPs is around 700 °C. A previously reported study from our group showed that this temperature range is crucial to the formation of Ni
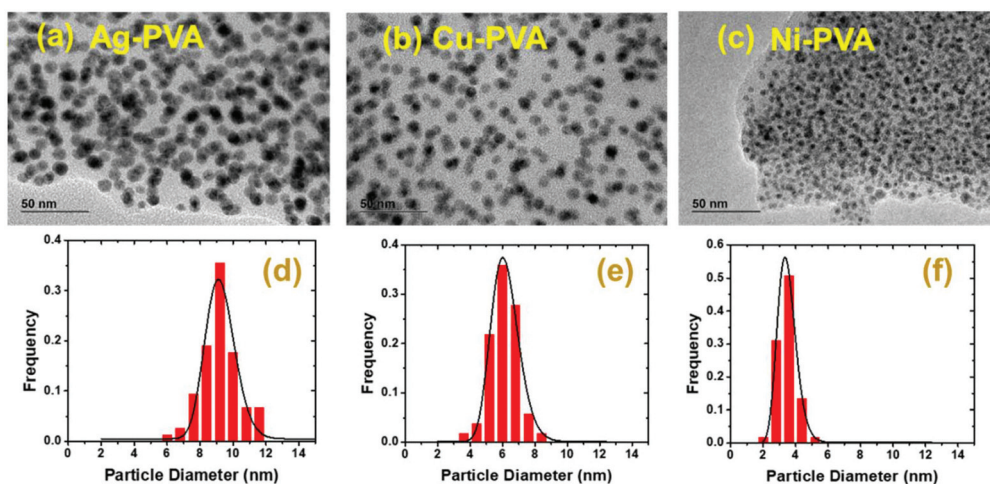
Fig. 2 (a), (b), (c) Formation of Ag, Cu, and Ni within the PVA matrix by the LPSW technique. Insets show selected area diffraction patterns for each sMNPs–PVA film. (d), (e), (f) Particle size distributions of Ag, Cu, and Ni respectively in PVA films (from a, b, c respectively). These films were coated on a 0.2 mm glass substrate.

Table 1 Parameters used to fabricate metal–PVA films shown in Fig. 2 by LPSW. These films were fabricated on 0.2 mm thick glass substrates

Metal	Metal : PVA mass ratio	Laser intensity (W cm^{-2})	Pulse duration	Number of pulses	Estimated peak film temperature (°C)	Chamber atmosphere
Ni	0.05 : 1	10	1 s	1	730	5% H$_2$ in N$_2$
Cu	0.05 : 1	2.5	4 s	1	640	5% H$_2$ in N$_2$
Ag	0.05 : 1	2.5	4 s	1	640	Ambient air

rather than NiO.[28] Although, even the Cu and Ag films reach similar peak temperatures, the heating rate is slower due to a lower energy flux, and hence, might not provide sufficient local thermal energy in time for Ni^{2+} reduction and Ni nanocluster formation. Previous studies have demonstrated that at high temperatures, the diffusion of gas molecules into polymer melts can be highly accelerated with diffusivities (D) as high as 10^{-4} cm^2 s^{-1}.[29] High diffusion rates are attributed to the higher mobility of polymer chains at elevated temperatures, allowing for the increased motion of gas molecules through microcavities and channels in the polymer matrix.[30] Using the diffusion equation,[31] $\langle x^2 \rangle = 2Dt$, we estimate the time ($t$) for H$_2$ molecules to diffuse through a 1 μm thick (x) polymer film to be ~50 μs, which is significantly faster than the fabrication timescale for Cu and Ni sMNPs (1–4 s). Furthermore, the first-order rate constants for the reduction of Cu and Ni salts by hydrogen at similar temperatures are estimated to be in the order of 10^2 s^{-1} and 10^0 s^{-1}, respectively.[32,33] Hence, the time for the half-conversion of Cu^{2+} and Ni^{2+} should roughly be in the order of 10 ms and 1 s, respectively. We, therefore, postulate that particle formation for these metals occurs by fast H$_2$ diffusion in the polymer, followed by a rapid reduction of metal ions.

Since H$_2$ diffusion in the matrix is fast, particle growth must not be limited by gas diffusion in the polymer. Interestingly, the mean particle diameters follow the trend (Ag: 9.0 nm, >Cu: 6.0 nm, >Ni: 3.5 nm). This observation

mirrors the reactivity trend for these metals (Ni > Cu > Ag). Studies have shown that more reactive metals have strong interactions with polymer chains that impede their diffusion through the matrix.[29] On laser heating, the large supersaturation of metal atoms results from fast reduction reactions. After this initial nucleation burst, out of the three metals, Ni atoms and clusters diffuse through the polymer the slowest. As these clusters grow larger, their motion is further retarded due to their increasing size. This limits particle growth and the maximum particle size reached for a particular laser pulse energy flux and duration, resulting in smaller Ni nanoclusters. Here, we also note that LPSW is not restricted to noble-metals and can be used to generate any metal given the right laser parameters and reduction conditions.

We have chosen Ag as the model metal to study the effect of laser parameters in LPSW on sMNP size distribution due to its relative ease of fabrication and highly size-sensitive visible localized surface plasmon resonance (LSPR). Ultrathin Ag–PVA films are fabricated by coating precursor–PVA thin films (~100 nm) with a thick (~20 μm), sacrificial PS film (method described earlier in the Experimental section) and are directly imaged through TEM to assess particle size distribution over a large area in the film. Although, LPSW can be used directly on freestanding polymer films to fabricate Ag–polymer composites (as we later demonstrate), we have used glass substrates to coat the polymer films on. This is done to ensure a uniform coating and to avoid variations in the laser–polymer

film alignment due to local curling and folding inhomogeneity in the polymer film. Note that, the films discussed so far were coated on 0.2 mm thick glass substrates, which allow the films to reach high temperatures by preventing significant conductive heat losses. In further sections, we have used thicker (1 mm) glass substrates, which act as conductive heat sinks and result in lower film temperatures. This was done to achieve faster quenching rates and to prevent additional film heating effects by the glass itself (ESI, section S5†). Laser energy manifests itself in the PVA film as heat and may have multiple sources: direct laser–PVA interaction by partial IR absorption by PVA itself, conductive heat transfers from the underlying PS film or glass substrate. In any case, this localized thermal energy is responsible for metal-ion reduction and particle formation.

An ideal, continuous laser synthesis and writing technique should be able to tune the particle size and properties by modulating laser characteristics. Here, we systematically investigate the effect of three primary laser characteristics on written particle size distribution: laser energy flux, pulse duration, and number of laser pulses of a fixed intensity and duration irradiating the films. In all of the following cases, the metal-precursor to polymer mass ratio is kept constant at 0.05 : 1, and 1 mm thick glass slides are used for the coating.

3.2. Effect of individual laser parameters on written particle size distribution

3.2.1. Laser pulse duration. For these experiments, the beam spot diameter (1 cm), and laser energy flux (20 W cm^{-2}) are kept constant, while the pulse duration is varied from 200 ms–1000 ms. Fig. 3(a) shows the variation of lognormally fit particle size distributions (PSD) with laser pulse duration. As is clear from size distributions (Fig. 3(b)), with increasing pulse duration, an increase in the mean particle diameter is observed ($D_{p, mean}$ increases from 4.2 nm to 9.5 nm). Interestingly, a concomitant decrease in PSD geometric standard deviation (σ_g) is also seen with increasing pulse duration (σ_g: 1.30 → 1.11). Note that, these σ_g values are still much lower than the coagulation-dominated self-preserving distribution (SPD) in the continuum regime ($\sigma_{g, SPD} = 1.44$). This suggests that the polymer film acts as a restrictive matrix that greatly suppresses particle coagulation. The decrease in PSD width (σ_g) suggests a mechanism dominated by surface growth or a form of digestive ripening.
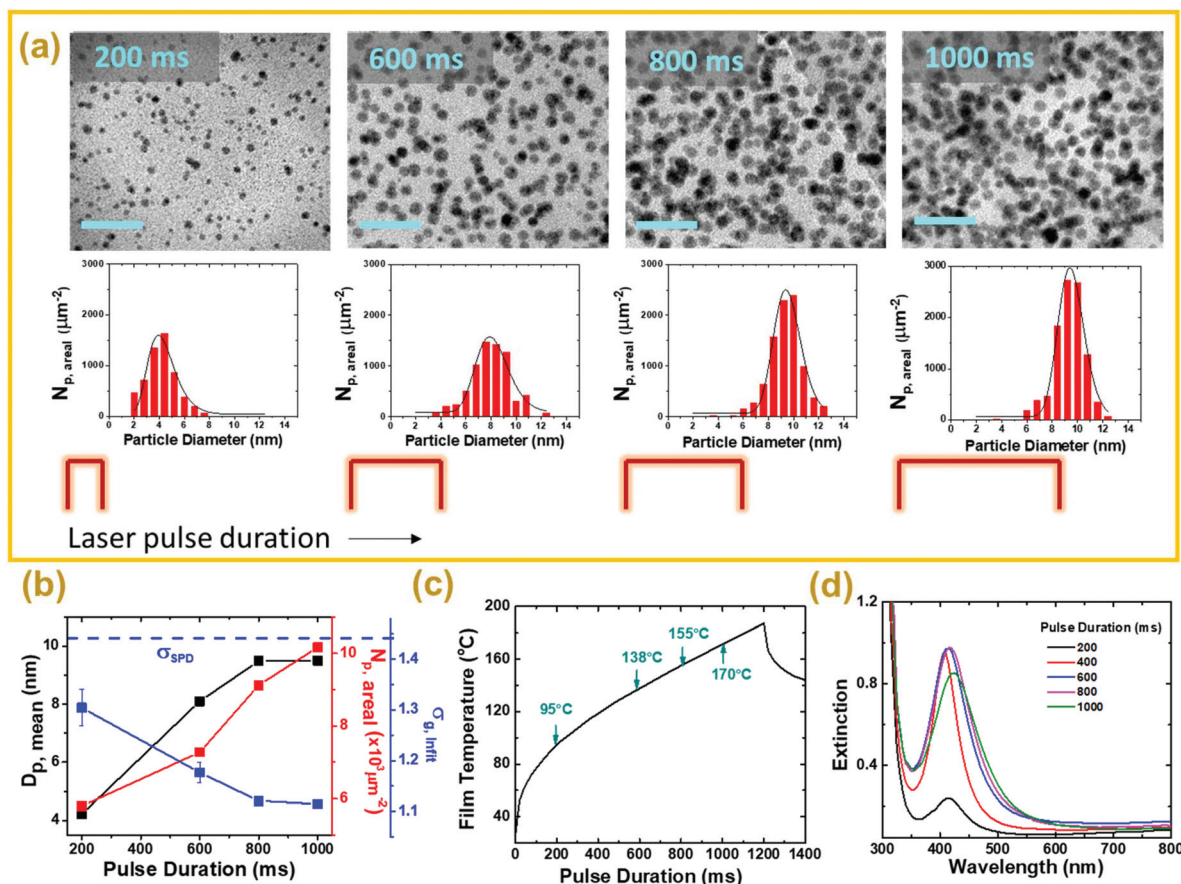
Fig. 3 (a) TEM images (scale bars: 50 nm) and the corresponding PSDs of Ag sMNPs−PVA films fabricated for different laser pulse durations for a fixed laser energy flux of 20 W cm^{-2}, (b) effect of pulse duration on the mean particle diameter, areal particle mass density, and geometric standard deviation ($\sigma_{g, lnfit}$) obtained from lognormally fit PSDs, (c) simulated temperature profile of the laser heating process with temperatures for durations shown in (a), (d) extinction spectra of Ag sMNPs−PVA films fabricated by LPSW. Substrate used is a 1 mm glass slide.

With the increase in pulse duration, the temperature and thermal energy in the polymer increases. Since the temperature to which polymer films are heated to is close to or above the glass transition temperature of poly(vinyl alcohol) (T_g = 85 °C),[34] the polymer matrix must be in a partly molten or "rubbery" state, allowing for high diffusion of metal ions, atoms, and clusters. It has been shown that for less reactive metals such as Ag, the diffusivity through polymer melts at or above T_g can be very high ($\sim 10^{-3}$ cm^2 s^{-1}). An initial burst nucleation results in a large supersaturation and formation of stable nuclei. The diffusion coefficient, D, is inversely proportional to the particle diameter (D_p) and matrix viscosity (η).[31] Small nuclei with higher diffusion coefficients diffuse through the matrix, grow by coagulation, and form larger primary particles. Increased temperature not only allows for faster diffusion by increasing the kinetic energy of the particles, but also by decreasing the viscosity of the surrounding polymer matrix. Simultaneously, the rate of the metal-ion reduction reaction and the corresponding increase in metal atoms increase exponentially with temperature. This leads to the continued surface growth of existing metal particles by metal atoms and small clusters. As particles grow by surface growth and ripening, the diffusion coefficient decreases – particularly for particles with a larger size. These mechanisms may, therefore, result in a decreasing PSD width.

Fig. 3(d) shows the effect of pulse duration on LSPR absorption of Ag sMNPs. Plasmonic absorption peaks for Ag sMNPs are extremely sensitive to the size, shape, and refractive index of the surrounding medium. Here, we assume that all LPSW fabricated Ag sMNPs are spherical (evidenced by TEM images), and that the polymer itself does not change its structure significantly.

Hence, the absorption peak shifts in the spectra can be correlated with changes in particle size distribution of sMNPs. An increasing laser intensity results in an initial increase in extinction. This can be attributed to nucleation – as more absorbing nuclei of a particular size are formed, absorption increases. An initial blue-shift followed by a red shift in the peak wavelength is observed. This kind of turn-over shift has been associated with the size increase in Ag sMNPs and a shift from extrinsic to intrinsic surface screening and spill-out effects in the sub-10 nm small NP size regime.[35] This observation correlates with the increase in diameter observed for these two films in the TEM images (Fig. 3(a)).

3.2.2. Laser energy flux. For these experiments, the beam spot diameter (1 cm), and laser pulse duration (1000 ms) are kept constant, while the laser energy flux is varied from 8–23 W cm^{-2}. Laser energy flux can be considered analogous to the heating rate in conventional heating techniques. Fig. 4(c) shows the temperature variation of PVA films with increasing energy flux. For a fixed pulse duration, a high-energy flux laser
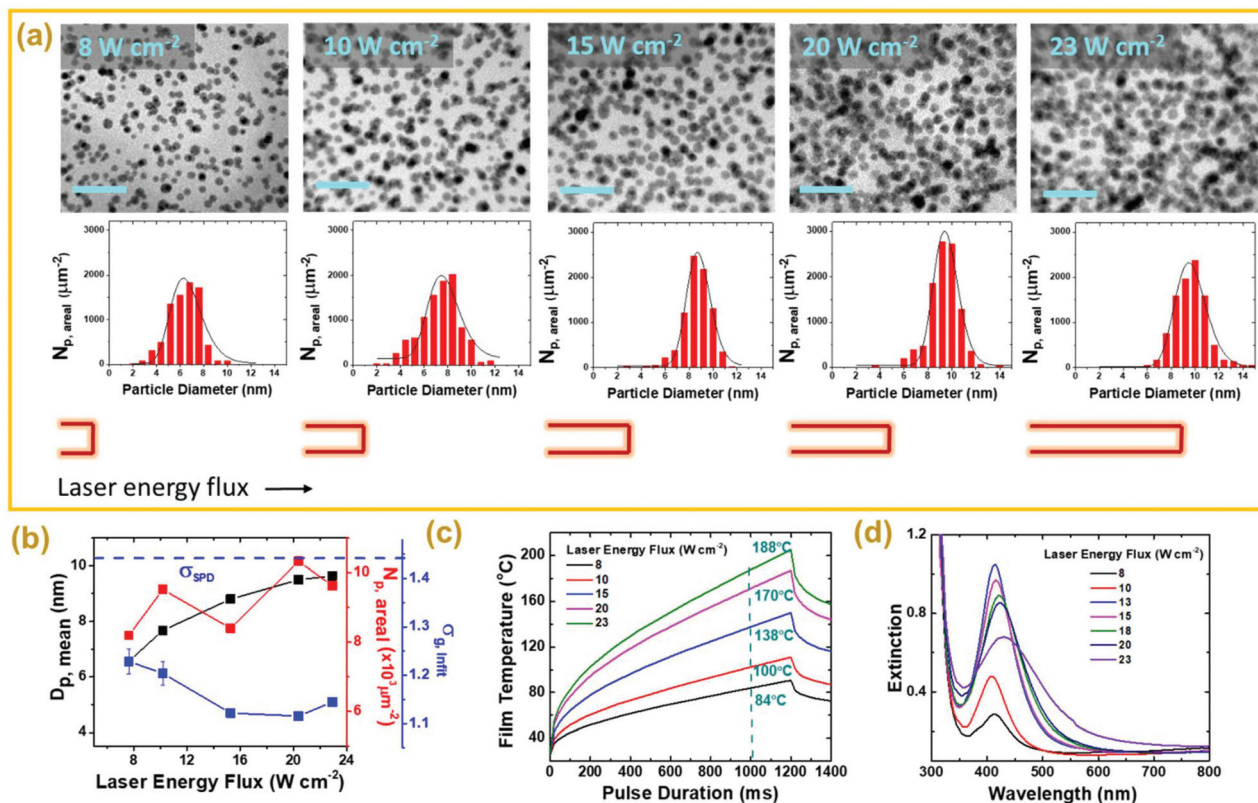

Fig. 4 (a) TEM images (scale bar: 50 nm) and the corresponding PSDs of Ag sMNPs−PVA films fabricated for different laser energy flux for a fixed pulse duration of 1000 ms, (b) effect of laser energy flux on the mean particle diameter and geometric standard deviation ($\sigma_{g, \ln fit}$) obtained from lognormally fit PSDs, (c) simulated temperature profile of the laser heating process with varying energy flux, (d) extinction spectra of Ag sMNPs−PVA films fabricated by LPSW for different laser energy flux. Substrate used is a 1 mm glass slide.

pulse ramps up the temperature of the polymer film faster. This not only generates more metal nuclei but also allows the nuclei to diffuse through the matrix and grow into larger particles. The particle diameter increases from 6.5 to 9.5 nm with a decrease in σ_g of the PSDs. This result is similar to the one obtained in the earlier section with increasing pulse duration, suggesting a similar digestive ripening growth mechanism. We compare the PSD of the 10 W cm^{-2}, 1000 ms film with 20 W cm^{-2}, 200 ms film (Fig. 3(a) and 4(a), respectively). These two pulses lead to roughly similar temperatures (95–100 °C) but have different heating rates with the former pulse being slower and longer than the latter. We observe that with slower and longer laser pulse, the particle size is larger, and the size distribution is narrower. This may be because a shorter pulse causes the processes occurring in the matrix – metal atom generation, nucleation, and diffusion – to be stochastic without allowing enough time for diffusion, particle growth, and PSD narrowing. Fig. 4(d) shows the trend in plasmonic absorption spectra for the films prepared with varying laser energy flux. The blue-shift to red-shift turn-over trend in the plasmonic peaks of the Ag sMNPs is again observed as in the earlier section. As mentioned earlier, this type of shift can be attributed to the size increase in the sub-10 nm size regime, where surface effects become significant.

3.2.3. Number of pulses: pulsed thermal load. For a pulse with the highest energy flux and longest pulse duration explored so far (23 W cm^{-2}, 1000 ms), slight agglomeration was observed as evidenced by the decrease in the areal number density and corresponding increase in the particle diameter (Fig. 3(a) and (b)). Additionally, at these temperatures, polymer films became brittle and flaky possibly due to charring and crystallization at high temperatures. In order to prevent these problems, we propose an alternative heating method using a periodic, pulsed heat load. We employ a significant and unique advantage of the LPSW technique over slow heating methods – the ability to generate programmable sets and sequences of high-energy flux pulses of any form. Individual characteristics of each pulse such as intensity and duration can be precisely controlled using a pulse generator. Exploiting this unique process of the LPSW, we investigated the effect of irradiating the films at the same spot with a set number of pulses of fixed energy flux and duration. In these experiments, a certain number of 20 W cm^{-2}, 200 ms pulses were exposed on the same spot of the metal precursor–PVA film. Each subsequent pulse was interspersed with a 15 s wait time for particles to fully recover from the heating effects of the preceding pulse. Fig. 5(b) demonstrates the temperature profile of the polymer during this heating process with an
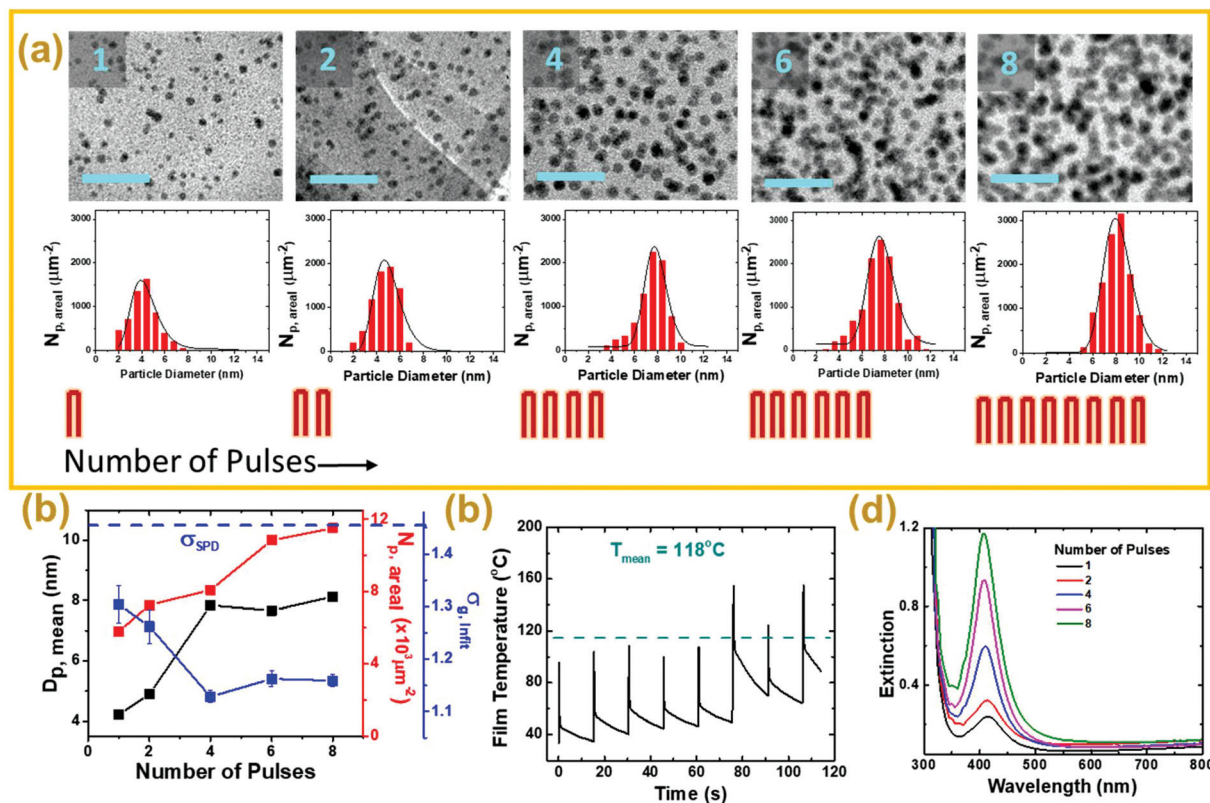

Fig. 5 (a) TEM images (scale bar: 50 nm) and the corresponding PSDs of Ag sMNPs–PVA films fabricated for different laser pulses; 20 W cm^{-2}, 1000 ms pulses, (b) effect of number of input pulses on the mean particle diameter and geometric standard deviation (σ_g) obtained from lognormally fit PSDs, (c) simulated temperature profile of the laser heating process with a periodic heat load, (d) extinction spectra of Ag sMNPs–PVA films fabricated by LPSW for different number of pulses. Substrate used is a 1 mm glass slide.

average temperature per pulse of 118 °C. Fig. 5(a) shows a significant initial increase in the particle size and a decrease in the PSD width. After 4 pulses, the particle diameter and σ_g of PSDs do not change significantly, while the areal number density continues to increase. A similar trend is observed in the extinction spectra of these films (Fig. 5(d)). As more pulses are impinged on the metal precursor–polymer film, there is an initial strong blue-shift which stays roughly unchanged after the 4th pulse. At the same time, we also observe an increase in extinction – possibly mirroring the increase in the areal number density.

3.3. Effect of the polymer matrix: fundamental growth mechanisms

So far, we have only considered how laser characteristics impact PSDs of sMNPs. Here, we discuss the role of the polymer matrix in determining the resultant particle size distributions. In earlier sections, we observe that after a certain point, the particle size does not change significantly, which we propose is due to the restrictive and diffusion-suppressing nature of the polymer matrix. Here, we investigate how increasing the laser pulse duration (constant energy flux of 20 W cm^{-2}) affects the particle size and distribution in a PVA matrix with a lower molecular weight (9k PVA, as opposed to 89k PVA we talked about so far). Fig. 6(a) shows TEM images and size distributions for the Ag–9k PVA films fabricated for different pulse durations. Clearly, we see a significantly faster increase in the particle size than for the 89k PVA film (Fig. 3(a)).

Interestingly, for a 200 ms pulse, the mean particle diameter for both matrices is roughly the same (4 nm), however, the particle size distribution is much narrower for the 9k PVA matrix. This may be attributed to a lower viscosity of the low MW polymer.[36] The low inherent viscosity may result in higher diffusion rates for smaller nuclei, resulting in a more homogeneous nucleation and narrow distribution than a restrictive matrix. Interestingly, the PSD geometric standard deviation, σ_g, increases with increasing pulse duration – a sharp contrast

to the 89k polymer matrix, where an opposite trend is seen. This suggests that a different growth mechanism is at play for polymer matrices with different molecular weights and viscosities. The plasmonic peaks in Fig. 6(c) also indicate a dramatic broadening of the peak with a significant portion red-shifted due to the formation of larger particles.

Here, it is also important to note that there might be variation in film thicknesses during spin coating due to different solution viscosities. Nevertheless, the particle size distribution changes are too large to be attributed solely to the thickness of the film. Furthermore, for 89k PVA, even at the highest laser energy flux and pulse durations, the particle sizes did not reach large sizes as in the case of 9k PVA. The major factor in determining the growth mechanism may be the viscosity of the polymer matrix itself. Fig. 7 illustrates the two primary con-
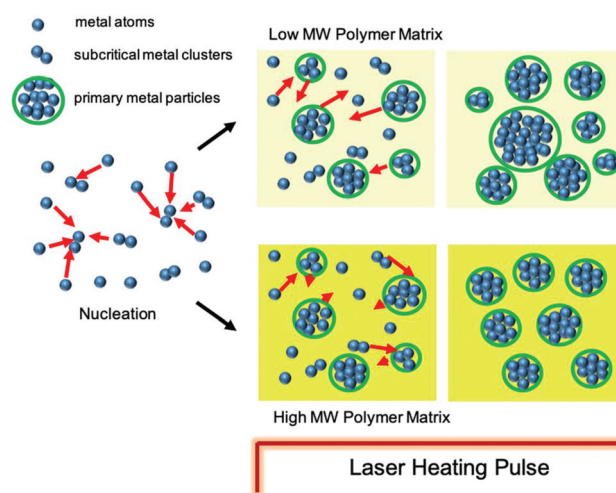

Fig. 7 Primary growth mechanisms in LPSW of metal particles in polymer matrices with different molecular masses, resulting in two different kinds of size distributions.
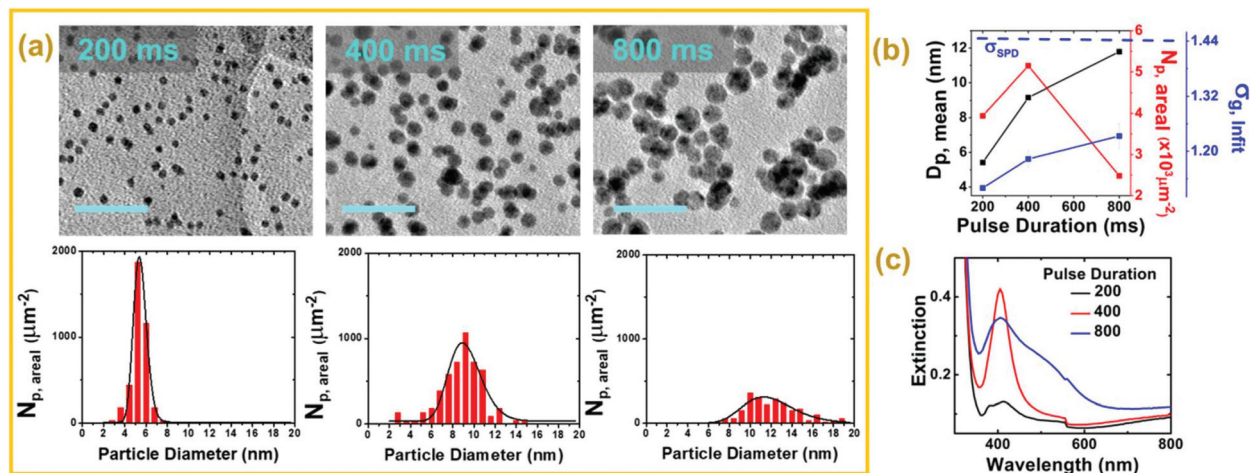

Fig. 6 (a) TEM images (scale bar: 50 nm) and the corresponding PSDs of Ag sMNPs–9k PVA films fabricated for different pulse durations for a laser energy flux of 20 W cm^{-2}, (b) effect of pulse duration on the mean particle diameter, geometric standard deviation (σ_g), and areal mass density in 9k PVA films, (c) extinction spectra of Ag sMNPs–PVA films fabricated by LPSW for different number of pulses. Substrate used is a 1 mm glass slide.

trasting mechanisms at play for the 9k and 89k polymer matrices. For a high MW polymer, the growth is restricted by the high-viscosity polymer melt which leads to a slower, limited growth and narrow PSDs. On the other hand, for a low-viscosity, low MW polymer film, diffusive growth is faster, such that the growth is partly coagulation dominated. Even larger particles are able to diffuse relatively quicker due to the low viscosity of the polymer matrix. This leads to a faster increase in the particle diameter and a concomitant increase in the width, σ_g, of the distribution. This observation is consistent with previously reported studies on polymer-encapsulated growth of Au and Fe nanoparticles.[37,38]

Furthermore, we also note that all the films discussed so far have a uniform dispersion of Ag sMNPs throughout the polymer matrix as shown in selected large-area TEM images (ESI, Fig. S5†).

3.4. Direct synthesis and writing of Ag sMNPs on free standing polymer films

We further investigated if our LPSW technique can be used directly on free standing polymer films. Fig. 8(a) and (b), show Ag sMNPs and corresponding PSDs fabricated by directly suspending a free standing PVA–PS film in the laser beam path. We noted using longer pulse durations discussed earlier (200 ms–1000 ms, Fig. 3) for free standing films damaged and burned them. In free standing films, there is no conductive heat sink, and the heating rate, therefore, is much more rapid. We, therefore, used an even shorter pulse duration (100 ms), and obtained a much larger mean particle diameter (9 nm) than that obtained for the films with the glass substrate

(4 nm, Fig. 3(a)). Temperature simulations in Fig. 8(c) also suggest a much faster heating rate without any substrate. We also see that there is a significant concentration of smaller nanoclusters in the film, which may be due to the short duration of the heating pulse. This may not give enough time for clusters to form bigger particles. Fig. 8(b) shows the plasmon peak for the freestanding film with the inset showing the character 'X' written by moving the polymer film. The yellow color in the film is due to the plasmon absorption by Ag sMNPs.

Importantly, Fig. 8(e) demonstrates the capability of our technique to fabricate Ag–sMNPs directly in a 30 μm thick, freestanding Ag precursor–PVA film (without PS or glass). Since PVA is a much stronger absorber than PS, an even shorter pulse duration of 35 ms was used to write the Ag sMNPs. Temperature simulations show average peak temperatures of around 360 °C. The inset in Fig. 8(c) depicts the writing of an arbitrary pattern (here, the acronym 'UMD') of sub-10 nm unaggregated Ag spheres directly in a polymer matrix. This pattern was obtained by moving the freestanding film with the laser pulses that is held in place on a sample holder. The yellow coloration is due to the plasmon absorption of Ag sMNPs. The non-uniform coloration in some parts is likely due to the overlapping of laser spots. Plasmonic spectra shown in Fig. 8(c) for selected non-overlapping spots in the three letters written confirm the formation of Ag sMNPs in the pattern. In addition, we also note that the lateral thermal diffusion and polymer damage during laser writing are minimal, which may be important when considering writing well-defined metallic patterns in the films (ESI, section S7†).
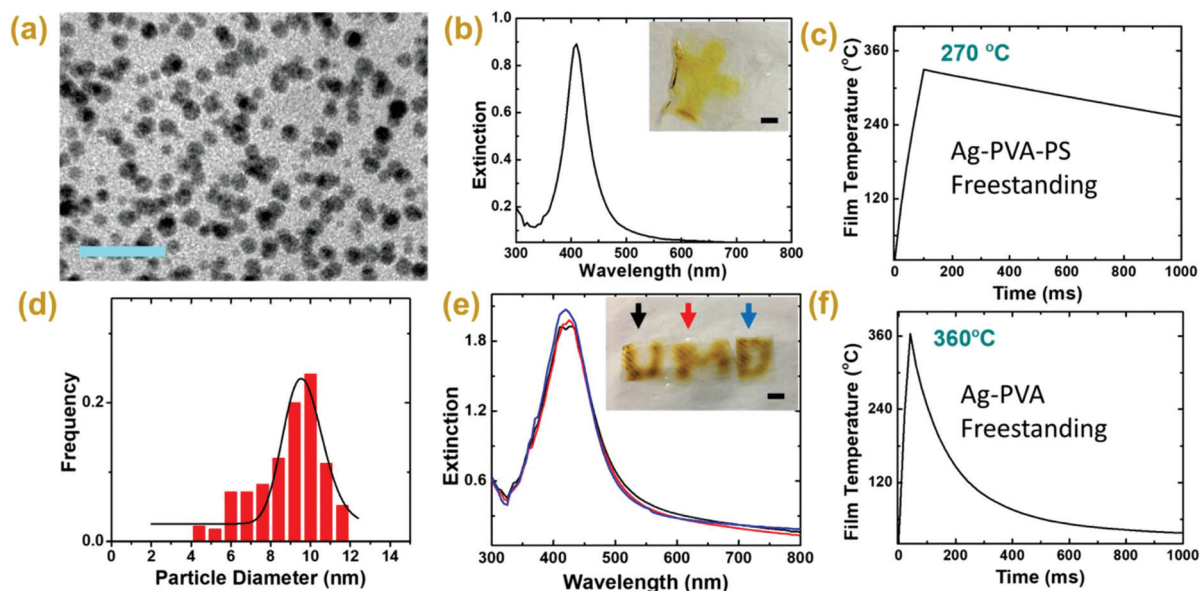
Fig. 8   (a) TEM images (scale bar: 50 nm) and (d) the corresponding PSDs of Ag sMNPs fabricated directly in freestanding PVA–PS films with a 20 W cm^{-2}, 100 ms pulse, (c) extinction spectra for the Ag–PVA–PS composite film shown in (a) – inset shows the letter 'X' written on the PVA–PS film by moving the film vertically and horizontally, (e) the letters 'U', 'M', 'D', written with Ag sMNPs by a 20 W cm^{-2}, 35 ms pulse directly on a thick, free standing PVA film, and extinction spectra in selected regions in the three individual letters (scale bar: 5 mm), (c), (f) simulated temperature profile for the freestanding film shown in (b), (e) respectively.

From known parameters, we can calculate the nanoparticle production rate for this process as follows. Using the film thickness and beam spot diameter, we can get the volume and mass of the polymer. Assuming all the metal salt in the heated volume is completed in 35 ms, we can calculate the mass of Ag produced per minute. Considering the continuous, direct laser synthesis approach of metal sMNPs in polymer films is amenable to fast and scalable polymer processing techniques such as roll-to-roll manufacturing and 3-D printing, we calculate the production rate to be around 1 g min^{-1} (ESI, section S6†), which is significantly higher than other conventional processes. Importantly, we further demonstrate that the written metal nanoclusters can be released into solutions by dissolving the polymer matrix in an appropriate solvent, making this approach solution-processable and comparable to colloidal synthesis (ESI, section S8†). Although the discussion above focusses primarily on mechanisms related to LPSW of Ag sMNPs, the effects of laser parameters on particle size distributions should apply to other metals (Cu, Ni) fabricated by LPSW as well.

4. Conclusions

In this study, we demonstrate laser photothermal synthesis and writing as a rapid laser writing technique that can be used to directly generate and write a high-density of unaggregated, monodisperse small metal nanoclusters in polymer thin films. In a relatively short time (35 ms–4s), a high-heating laser beam photothermally triggers metal-reduction reactions followed by nucleation and growth. Subsequent rapid quenching solidifies the polymer film and freezes the formed particles in the solid matrix. We have used this technique to write three types of metal nanoclusters (Ni, Cu, and Ag) in the film. We have further shown how laser parameters – laser energy flux, pulse duration, and number of pulses – can be used to tune the particle size distribution of metal nanoclusters in the films. Higher laser energy flux and pulse durations lead to an increase in the particle size with a corresponding decrease in the PSD width. Additionally, we demonstrate that multiple pulses of a fixed intensity and pulse duration can be used to modulate PSDs without damaging the polymer. We demonstrated that this synthesis can be adapted to different substrates as well as in free standing polymer films. Thus, this technique is a fast, continuous laser writing technique that is flexible and can be used to generate different metal nanoclusters in virtually any polymer matrix as long as it is partly absorbing in the mid-IR laser wavelength. We further note that LPSW may have significant implications in large-scale, rapid direct writing (1 g min^{-1}) of metal nanoclusters in advanced polymer matrices, reactive multilayers, conductive polymer films, wearable electronics, and flexible sensor films.

Conflicts of interest

There are no conflicts to declare.

References

1 X. Zhou, W. Xu, G. Liu, D. Panda and P. Chen, *J. Am. Chem. Soc.*, 2010, **132**, 138–146.

2 K.-S. Lee and M. A. El-Sayed, *J. Phys. Chem. B*, 2006, **110**, 19220–19225.

3 W. Zhu, R. Michalsky, Ö. Metin, H. Lv, S. Guo, C. J. Wright, X. Sun, A. A. Peterson and S. Sun, *J. Am. Chem. Soc.*, 2013, **135**, 16833–16836.

4 Y. Yang, P. Ghildiyal and M. R. Zachariah, *Langmuir*, 2019, **35**, 3413–3420.

5 L.-Y. Chen, C.-W. Wang, Z. Yuan and H.-T. Chang, *Anal. Chem.*, 2015, **87**, 216–229.

6 M. Rai, A. Yadav and A. Gade, *Biotechnol. Adv.*, 2009, **27**, 76–83.

7 M. C. Rehwoldt, Y. Yang, H. Wang, S. Holdren and M. R. Zachariah, *J. Phys. Chem. C*, 2018, **122**, 10792–10800.

8 Q. Yu, P. Gao, K. Y. Zhang, X. Tong, H. Yang, S. Liu, J. Du, Q. Zhao and W. Huang, *Light: Sci. Appl.*, 2017, **6**, e17107.

9 L. Shang and S. Dong, *J. Mater. Chem.*, 2008, **18**, 4636–4640.

10 S. Devarajan, P. Bera and S. Sampath, *J. Colloid Interface Sci.*, 2005, **290**, 117–129.

11 L. Rodríguez-Sánchez, M. C. Blanco and M. A. López-Quintela, *J. Phys. Chem. B*, 2002, **104**, 9683–9688.

12 T. Fujimoto, S. Terauchi, H. Umehara, I. Kojima and W. Henderson, *Chem. Mater.*, 2002, **13**, 1057–1060.

13 T. Herricks, J. Chen and Y. Xia, *Nano Lett.*, 2004, **4**, 2367–2371.

14 H. Dong, Y.-C. Chen and C. Feldmann, *Green Chem.*, 2015, **17**, 4107–4132.

15 D. Muñetón Arboleda, J. M. J. Santillán, L. J. Mendoza Herrera, M. B. F. van Raap, P. Mendoza Zélis, D. Muraca, D. C. Schinca and L. B. Scaffardi, *J. Phys. Chem. C*, 2015, **119**, 13184–13193.

16 S. A. Davari, J. L. Gottfried, C. Liu, E. L. Ribeiro, G. Duscher and D. Mukherjee, *Appl. Surf. Sci.*, 2019, **473**, 156–163.

17 Y. Liu and M. Lee, *ACS Appl. Mater. Interfaces*, 2014, **6**, 14576–14582.

18 P. Kunwar, J. Hassinen, G. Bautista, R. H. A. Ras and J. Toivonen, *ACS Nano*, 2014, **8**, 11165–11171.

19 S. Kang, K. Vora and E. Mazur, *Nanotechnology*, 2015, **26**, 121001.

20 V. K. Rao and T. P. Radhakrishnan, *ACS Appl. Mater. Interfaces*, 2015, **7**, 12767–12773.

21 S. Porel, N. Venkatram, D. N. Rao and T. P. Radhakrishnan, *J. Appl. Phys.*, 2007, **102**, 033107.

22 S. Ghosh, S. Bera, S. Bysakh and R. N. Basu, *ACS Appl. Mater. Interfaces*, 2017, **9**, 33775–33790.

23 S. Porel, S. Singh, S. S. Harsha, D. N. Rao and T. P. Radhakrishnan, *Chem. Mater.*, 2005, **17**, 9–12.

24 S. Porel, N. Venkatram, D. N. Rao and T. P. Radhakrishnan, *J. Nanosci. Nanotechnol.*, 2007, **7**, 1887–1892.

25 G. V. Ramesh, S. Porel and T. P. Radhakrishnan, *Chem. Soc. Rev.*, 2009, **38**, 2646–2656.

26 N. Sahba and T. J. Rockett, *J. Am. Ceram. Soc.*, 1992, **75**, 209–212.

27 S. T. Yang, M. J. Matthews, S. Elhadj, D. Cooke, G. M. Guss, V. G. Draggoo and P. J. Wegner, *Appl. Opt.*, 2010, **49**, 2606.

28 Y. Yang, M. Romano, G. Feng, X. Wang, T. Wu, S. Holdren and M. R. Zachariah, *Langmuir*, 2018, **34**, 585–594.

29 F. Faupel, R. Willecke and A. Thran, *Mater. Sci. Eng., R*, 1998, **22**, 1–55.

30 N. F. A. van der Vegt, *Macromolecules*, 2000, **33**, 3153–3160.

31 A. Einstein, *Ann. Phys.*, 1905, **322**, 549–560.

32 K. V. Van and F. Habashi, *Can. J. Chem. Eng.*, 1974, **52**, 369–373.

33 D. T. Williams, S. K. El-Rahaiby and Y. K. Rao, *Metall. Trans. B*, 1981, **12**, 161–166.

34 B. Sarti and M. Scandola, *Biomaterials*, 1995, **16**, 785–792.

35 S. Peng, J. M. McMahon, G. C. Schatz, S. K. Gray and Y. Sun, *Proc. Natl. Acad. Sci. U. S. A.*, 2010, **107**, 14530–14534.

36 J. F. Voeks, *J. Polym. Sci.*, 1959, **36**, 333–339.

37 R. G. Shimmin, A. B. Schoch and P. V. Braun, *Langmuir*, 2004, **20**, 5613–5620.

38 F. He and D. Zhao, *Environ. Sci. Technol.*, 2007, **41**, 6216–6221.